Lysophosphatidylcholine modulates the aggregation of human islet amyloid polypeptide

Yanting Xing,[†] Emily H. Pilkington,[‡] Miaoyi Wang,[‡] Cameron J. Nowell,[¶] Aleksandr Kakinen,[‡] Yunxiang Sun, [†] Bo Wang,[†] Thomas P. Davis,[‡§] Feng Ding[†*] and Pu Chun Ke[‡*]*

[†]Department of Physics and Astronomy, Clemson University, Clemson, SC 29634, USA

[‡]ARC Centre of Excellence in Convergent Bio-Nano Science and Technology, Monash Institute of Pharmaceutical Sciences, Monash University, 381 Royal Parade, Parkville, VIC 3052, Australia

[¶]Monash Institute of Pharmaceutical Sciences, Monash University, 381 Royal Parade, Parkville, VIC 3052, Australia

[§]Department of Chemistry, University of Warwick, Gibbet Hill, Coventry, CV4 7AL, United Kingdom

Corresponding Author

[*] Thomas P. Davis: thomas.p.davis@monash.edu, Feng Ding: fding@clemson.edu and Pu Chun Ke: pu-chun.ke@monash.edu.

ABSTRACT. Amyloid aggregation of human islet amyloid polypeptide (IAPP) is a hallmark of type 2 diabetes (T2D), a metabolic disease and a global epidemic. Although IAPP is synthesized in pancreatic β-cells, its fibrils and plaques are found in the extracellular space indicating a causative transmembrane process. Numerous biophysical studies have revealed that cell membranes as well as model lipid vesicles promote the aggregation of amyloid-β (associated with Alzheimer's), α-synuclein (associated with Parkinson's) and IAPP, through electrostatic and hydrophobic interactions between the proteins/peptides and lipid membranes. Using a thioflavin T kinetic assay, transmission electron microscopy, circular dichroism spectroscopy, discrete molecular dynamics simulations as well as free energy calculations here we show that micellar lysophosphatidylcholine (LPC), the most abundant lysophospholipid in the blood, inhibited the amyloid aggregation of IAPP through nonspecific interactions while elevating the α-helical peptide secondary structure. This surprising finding suggests a native protective mechanism against IAPP aggregation *in vivo*.

TOC GRAPHICS

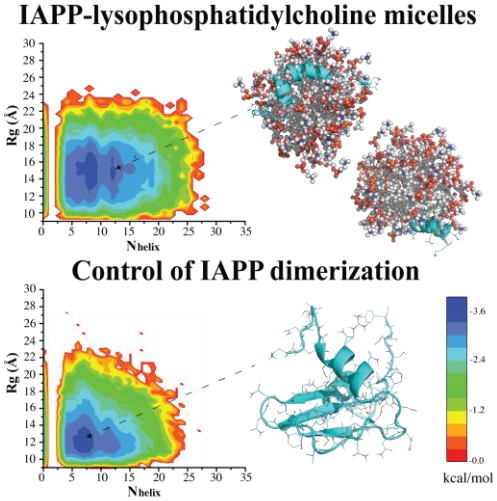

Micellar lysophosphatidylcholine inhibits the aggregation of human islet amyloid polypeptide (IAPP).

KEYWORDS. Amyloid aggregation · IAPP · membrane · inhibition · micelle

Introduction

Human islet amyloid polypeptide (IAPP) is an endocrine hormone that, in its monomeric form, regulates glucose metabolism in cooperation with insulin. However, IAPP is aggregation prone sans the stabilisation of insulin, physiological metal ions, low pH,[1-6] or their complexation with zinc and C-peptide,[7] and accumulating evidence has implicated IAPP amyloid aggregation as a hallmark of pancreatic β-cell death and type-2 diabetes (T2D), a disease impairing millions of people worldwide with profound social and economic implications.

IAPP is synthesised in pancreatic β-cells and co-released with insulin to blood circulation for glycemic control.[1] IAPP fibrils and plaques, however, appear in the extracellular space of the Langerhans suggesting a role of cell membranes in inducing aberrant IAPP aggregation. Indeed it has been shown in the literature that cell membranes as well as lipid vesicles generally promote IAPP aggregation,[8-19] as also observed for amyloid-β and α-synuclein in neurodegenerative disorders.[20,21] Conversely, IAPP disrupts membrane integrity through lipid extraction or pore formation.[13,15,19,20] On the molecular level, the binding between IAPP and a lipid interface is initiated by the N-terminus of the peptide, through electrostatic interaction with the anionic lipids and facilitated by hydrophobic interaction engaging the lipid bilayer and the amphiphilic peptide oligomers, protofibrils and fibrils.[8-12,14] Among these, oligomeric IAPP has been widely acknowledged as the toxic species based on *in vitro* and animal studies.[1,8]

Upon release into the bloodstream IAPP is exposed to a myriad of plasma proteins and lipids, yet the impact of such exposure on IAPP conformation and toxicity has rarely been studied. Recently we have proposed the concept of protein corona for elucidating the physicochemical and structural transformations of IAPP in circulation.[22] In this study we examined the effects of zwitterionic

lysophosphatidylcholine (LPC) at both below and above its critical micelle concentration (CMC, 40-50 μM)[23] on IAPP aggregation. LPC is the most abundant single-tailed phospholipid in the blood (234 μM)[24] as well as a signaling molecule in the cell membrane. At concentrations above the CMC, such as in the blood, LPC molecules render ultra-small micelles (~4 nm in diameter)[25,26] in size similar to that of sodium dodecyl sulfate (SDS). From the perspective of a model membrane the zwitterionic LPC micelles mimic the largely neutral pancreatic β-cell membranes (97.5% neutral, plus 2.5% anionic lipids)[27] more closely than the anionic SDS that has been used as a model system for examining protein-membrane interactions.

The fibrillisation of IAPP in the presence of linear and micellar LPC was quantified by a thioflavin T (ThT) kinetic assay and high-resolution transmission electron microscopy (TEM). The changing secondary structure of IAPP in the presence of linear and micellar forms of the lipid was probed with circular dichroism (CD) spectroscopy. A surprising inhibition effect of LPC micelles on IAPP amyloid aggregation was revealed, characterized by a prolonged lag time, a reduction in the β-sheet content at saturation, and sparse formation of soft, braided IAPP fibrils. Atomistic discrete molecular dynamic (DMD) simulations[28] were performed to provide molecular details of IAPP-LPC interaction. Upon binding the micelles, the C-terminal region of IAPP that is unstructured in solution[29] started to adopt an α-helical conformation. The hydrophobic interfaces of the amphiphilic N- and C-terminal helixes were buried at the lipid head-tail interface, forming a well-defined IAPP-micelle complex to inhibit the self-association and aggregation of IAPP.

Results and discussion

Effects of LPC binding on IAPP fibrillisation and remodelling - experiments

Biophysical characterisations revealed the differential effects of micellar and non-micellar LPC on IAPP fibrillisation, and additionally, their capacities in remodelling of mature IAPP amyloids (Fig. 1). Native fibrillisation of IAPP, which forms long, semi-flexible amyloid fibrils in aqueous solution over 24 h, was notably inhibited by micellar LPC (Fig. 1B). ThT fluorescence indicated a reduction in the β-sheet content formed by IAPP in the presence of micellar LPC by 24 h, compared to the IAPP control (Fig. 1A). Non-micellar LPC induced a lag time of only ~10 min and the saturation point was reached ~2 h before the IAPP control. This effect has also been observed with the Alzheimer's-related amyloid-β, where LPC below the CMC was capable of reducing the fibril lag and elongation times of amyloid-$\beta_{1\text{-}42}$, yet showed no notable increase in fibrillisation after saturation was reached in each case.[30] Anionic non-micellar lipids, including SDS[31] and lysophosphatidic acid (LPA)[32], have demonstrated the capacity to promote fibrillisation and fibril elongation of β_2-microglobulin (β2M) at a neutral pH, though zwitterionic LPC did not mediate any significant effect.

The interaction of micellar LPC with IAPP, in contrast, greatly reduced IAPP fibrillisation, both in terms of fibrillisation kinetics and overall amyloid formation by 24 h. CD spectroscopy revealed the transition of peptide secondary structure from random coils to β sheets over 24 h (Fig. 1C). In the presence of non-micellar LPC, an increase in β-sheet content of ~15% was observed for IAPP by 24 h, while the α-helical content (< 10%) showed negligible variations over the experimental period. In contrast, interactions of IAPP with LPC micelles induced an immediate transition from β sheets to α helices (39.2%). Within the IAPP-LPC micelle complex, IAPP random coils remained stable over 24 h (~33%). In contrast, Patil *et al.* observed that upon complexation with SDS micelles, IAPP residues 5-28 were present in the α-helical conformation, with residues 5-19

embedded in the hydrophobic core, and the known amyloidogenic region (residues 20-29) positioned on the surface of the micelle at the lipid-solvent interface.[14]

Given the limited capacity for inter-peptide interactions between micelle-bound IAPP, disruption of IAPP fibrillisation is expected. Indeed, visualisation of IAPP amyloid fibrils after 24 h in aqueous solution demonstrated significant structural polymorphism of IAPP fibrils in the presence of micellar LPC by TEM imaging (Fig. 1B) and subsequent analysis of fibril diameter (Fig. 1D). Large, braided amyloid fibrils larger than 30 nm in diameter were observed (Fig. 1B), displaying a significantly broadened distribution compared with the IAPP control or IAPP treated with non-micellar LPC (Fig. 1D), though fewer fibrils were seen. The fibrils appeared softer, with a persistence length of 458 ± 13 nm based on FiberApp statistical analysis,[33] compared with that of 2,885 ± 60 nm for the IAPP control.[34] Below the CMC, LPC remodelled amyloid fibrils into filaments of thinner width (Fig. 1D). Micellar LPC (Fig. S1, 4-5 nm in size) did not remodel pre-formed fibrils, but similarly to their effect on fibrillating IAPP, individual fibrils were observed to closely associate, belying the 'glue-like' effect of LPC micelles on mature amyloids.

Effects of LPC binding on IAPP structure by discrete molecular dynamics simulations

Micellar LPC inhibits IAPP aggregation. Each LPC micelle comprised of 50 LPC lipid monomers was pre-assembled and equilibrated by DMD simulations, rendering a micellar diameter of ~4 nm (Methods). Simulations of IAPP peptides and LPC micelles were performed at a 2:2 ratio to investigate the effect of LPC micelles on IAPP self-association. The control simulations of two IAPPs alone were carried out at the same concentration. Averaging over 20 independent simulations, the self-association of IAPP was monitored by computing the average number of atomic contacts between the two IAPPs as well as the binding between the IAPP and the micelle as a function of time (Fig. 2A). Indeed, the self-association of IAPPs was significantly

reduced (Fig. 2A, upper panel) due to their higher tendency to bind micelles (Fig. 2A, lower panel). To characterise the interactions of LPC micelles with IAPP, the binding frequency of each IAPP residue with either the hydrophobic tails or hydrophilic heads of LPCs was calculated (Fig. 2B). The hydrophobic tails of LPCs in the micelle core preferentially bound to the hydrophobic residues of IAPP, i.e., L12, F15, L16, F23, I26, L27 and Y37 (Fig. 2B inset). The hydrophilic residues of IAPP had higher binding frequencies with the phosphorylcholine heads of LPCs than their hydrophobic tails, indicating a stable IAPP-micelle complex formation by burying the hydrophobic IAPP residues into the hydrophobic core of the LPC micelle and exposing the hydrophilic IAPP residues on the surface. In the presence of LPC micelles, the overall helical content of IAPP increased while the β-strand and turn contents decreased compared to IAPPs alone (Fig. 2C), which is consistent with the CD experiment (Fig. 1C). In particular, the increased α-helix propensities were mainly in residues 18-29, approximately corresponding to the IAPP amyloidogenic region (Fig. 2D).[35] To better characterise the structural properties of IAPPs in the presence and absence of LPC micelles, a two-dimensional potential of mean force (2D-PMF, or effective free energy) was computed with respect to the radius of gyration (*Rg*) and the number of residues in helix conformations (N_{helix}) (Fig. 2E, 2F), $PMF = -K_B T ln P(R_g, N_{helix}) + C$, where K_B is the Boltzmann constant, T the simulation temperature at 300 K, and C a constant set to render the lowest PMF value at zero. Compared to the control simulations of an IAPP dimer, the energy basins of IAPPs in the presence of LPC micelles shifted toward larger N_{helix} values with a new basin emerging at N_{helix} ~12 and larger *Rg* values. By burying the hydrophobic residues of the amphiphilic helices at the N- and C-termini in the micelle, IAPPs became extended on the micelle surface, while IAPPs alone formed a more compact dimer structure stabilised by inter-chain hydrogen bonds and hydrophobic interactions (snapshots in the inset of Fig. 2E, 2F corresponding

to the indicated PMF basins). The simulations suggest that LPC micelles prevented IAPP self-association and aggregation by stabilising IAPP monomers in the IAPP-micelle complexes. In addition, the small size of LPC micelles and their correspondingly large curvature also stabilised the surface-bound IAPPs in the monomeric form, hence preventing formation of β-sheet rich amyloid fibrils due to the geometric impartibility between a flat β-sheet and the highly curved binding surface.

Soluble LPCs promote IAPP self-association. The effect of LPC monomers on IAPP self-association was examined by simulating the self-assembly of six IAPP peptides in the presence and absence of 24 initially isolated LPC molecules (Methods). To quantify the self-association of IAPPs, a single-linkage clustering analysis of snapshot structures along the simulation trajectories was performed: two molecules formed a cluster if they were in contact (i.e., making at least one intermolecular contact) and a molecule belonged to a cluster if it was in contact with any of the member molecules. In the presence of LPCs, the average number of IAPP-containing clusters rapidly dropped from 6 to 2 while the control simulations still had ~4 clusters after 200 ns (Fig. 3A). Using the last 25 ns of all simulations, we compared the distribution of mass-weighted IAPP cluster sizes in the presence and absence of initially isolated LPC monomers, where the presence of LPC monomers enhanced the self-association of IAPPs for larger oligomers (Fig. 3B). Compared to LPC micelles, these initially isolated LPCs had similar binding profiles to IAPP residues, but with overall stronger hydrophobic interactions (Fig. 3C) due to a higher accessible hydrophobic surface per lipid. The snapshots from 6 IAPPs with initially isolated LPCs illustrated the process of co-aggregation of IAPPs with LPCs (Fig. 3D). IAPP initially bound to one or several LPCs due to strong hydrophobic interaction and formed small and then large IAPP-LPC complexes with increased hydrophobic surfaces (150 & 200 ns; Fig. 3D). Therefore, these results suggest that

the presence of LPC monomers accelerated the self-association of IAPPs. Since the timescales accessible to atomistic DMD simulations were much shorter than the aggregation kinetics in experiments, no significant changes in IAPP secondary structure were observable with and without LPCs (data not shown).

Binding of LPC with IAPP amyloid fibril. The binding of LPC lipids with a two-layered IAPP amyloid fibril was examined. The fibril model consisted of 40 peptides (Fig. S3), reconstructed based on solid-state NMR constraints (Methods).[36] 30 independent simulations of 160 LPC monomers with randomly assigned initial positions and orientations around the fibril were performed, where the model fibril was fixed and LPCs were allowed to move freely. The distributions of LPC clusters in solution and bound to the fibril were calculated (Fig. 4A). In solution, the lipids self-assembled into various clusters or micelles with still isolated monomers. LPC could also bind the fibril and form larger clusters on the fibril surface (e.g., the large cluster of ~100 LPCs in the inset of Fig. 4A). The binding profile of LPCs with different IAPP residues in the fibril (Fig. 4B) was highly selective compared to free IAPPs (Figs. 2D & 3C). Interestingly, residues with high binding frequencies to LPCs formed four consecutive surface patches on the fibril surface or two LPC binding sites due to the two-fold symmetry of the fibril along the axis. One of the binding sites was around hydrophobic residues L12, F15, V17, and H18, forming a flat hydrophobic surface patch on the fibril surface (Fig. 4C). A large amount of LPCs bound to this site (i.e., the largest LPC cluster of ~100 lipids in Fig. 4A) and formed a half-worm like morphology. LPC monomers could fit onto the groves between two consecutive β-strands (e.g., LPCs highlighted in spherical representation in Fig. 4C). The other binding site (formed by residues N3, A5 and Y37) was smaller and curved and the bound LPCs remained in the micelle morphology (Fig. 4D). Although simulations with the fibril fixed could not capture remodeling of

the fibril by LPCs, the strong LPC-fibril binding suggests that LPC could coat the fibril and bundle multiple fibrils into a braided structure as observed in TEM (Fig. 1B). This can also explain the slightly reduced ThT intensity but increased β sheet content observed for IAPP fibrillisation in the presence and absence of LPC < CMC (Fig. 1A vs. 1C, middle panel), as the strong binding of LPC monomers onto IAPP fibrils and protofibrils would sterically hinder ThT dye from binding thereby reducing its fluorescence. The combined ThT, CD, TEM and DMD results suggest that LPC monomers accelerated IAPP binding.

Conclusion

The uncovered phenomenon of IAPP aggregation inhibition by micellar LPC offers a new mechanism to the existing models of IAPP stabilisation by insulin, low pH, metal ions,[1] or by zinc-C-peptide-IAPP complexation.[7] Interestingly, although not directly related to this study, it has been shown in the literature that whey protein α or β caseins, usually present in the form of micelles through mutual hydrophobic and electrostatic interactions, show a chaperone-like activity in inhibiting amyloid beta and insulin from aggregation through mechanisms not yet understood.[37,38] Differently from cell membranes and SDS micelles that are net negative, zwitterionic LPCs readily disperse in water as ultrasmall micelles and subsequent interact with IAPP to halt the latter's aggregation. Lastly, some LPC species are nearly 5 times more concentrated in the β-cell secretory granules compared to the rest of the cell, and are downregulated some 40-60% after glucose stimulation[39] suggesting a connection between LPC abundance and IAPP activity. These unique physicochemical characteristics of LPC may be crucial to IAPP stabilisation *in vivo* and instructive to the design and development of small molecules and nanoparticles against amyloidosis.

Materials and Methods

Materials

Human islet amyloid polypeptide (IAPP; 37 residues, 2-7 disulfide bridge, 3.9 kDa, >95% pure by HPLC) was obtained in lyophilised monomeric form from AnaSpec, and prepared in Milli-Q water at a stock concentration of 200 μM at room temperature with mixing immediately prior to use. Mature IAPP amyloids were aqueous solutions of IAPP incubated for more than 24 h. Thioflavin T (ThT) dye and L-α-Lysophosphatidylcholine (LPC; from *Glycine max,* >99% pure by TLC) were purchased from Sigma-Aldrich. LPC derived from soybean is primarily composed of unsaturated C-18 fatty acids; typically 40-60% linoleic, 25-30% palmitic, 10-12% oleic, 7-10% stearic and 4-6% linolenic acid.

Thioflavin T (ThT) assay

IAPP alone (25 μM) or in the presence of micellar and non-micellar LPC was mixed with 25 μM ThT dye in a black/clear bottom 96-well plate (Costar), with the remaining volume made up to 100 μL with Milli-Q water where necessary. ThT fluorescence (Excitation: 440 nm/ Emission: 485 nm) was then read every 10 min for 24 h (144 time points) on an EnVision plate reader (Perkin Elmer). Error represents the standard error of mean of two independent experiments. Data was fit to a sigmoidal curve (least squares) using Prism (GraphPad).

Transmission electron microscopy (TEM) and analysis

Carbon-coated formvar copper grids (400 mesh, ProSciTech) were glow discharged to promote hydrophilicity. A 10 μL aliquot of IAPP (25 μM) in the presence or absence of LPC was placed on the grid and allowed to adsorb for 60 s. The remaining solution was then drawn off and the grid washed twice in 10 μL of Milli-Q water. The grid was then touched to 5 μL 1% uranyl acetate (in

Milli-Q water), the solution immediately drawn off, and the grid then placed onto a 5 μL droplet of 1% uranyl acetate to stain for 15 s. Any remaining liquid was then drawn off and the sample allowed to dry. Grids were imaged using Tecnai TF20 (FEI) and JEOL 2000FX transmission electron microscopes. Fibril diameter analysis was undertaken using GMS 3 (Gatan), with the sample size as 150 data points. Statistical analysis was performed with Prism (GraphPad), utilising a one-way ANOVA with Tukey's correction. Statistical significance was determined as $p < 0.05$.

Circular dichroism (CD) spectroscopy

Experiments were performed on a Chirascan CD spectrometer (Applied Photophysics), with spectra read from 190-260 nm. Prior to sample loading, a baseline with no cuvette was run. 300 μL of 25 μM IAPP in Milli-Q water, alone or in the presence of LPC above (2 mM) and below (25 μM) the CMC, was placed in a cuvette with a 0.1 cm pathlength and CD analysis was run at 0 h, 2.5 h and 24 h time points. Between samples, cuvettes were washed more than 5× with distilled water. Reads are an average of 3 repeats. Raw data were offset to zero and normalized against the spectra of Milli-Q water for IAPP spectra, and against LPC alone at each respective concentration for IAPP-LPC mixed samples (Fig. S2). Data were then de-convoluted with CDNN software to give a final relative percentage content of secondary structure.

Discrete molecular dynamics (DMD) simulations

DMD is a special type of molecular dynamics algorithm where conventional continuous potentials are replaced by optimized step-wise potential functions.[40,41] A more comprehensive description of the DMD algorithm was published elsewhere.[27] In brief, the united-atom model represents all molecules where all heavy atoms and polar hydrogen atoms are explicitly modeled. An implicit solvent model was adopted in our system. The interatomic interactions included *van der Waals*, solvation, electrostatic interactions and hydrogen bond. The solvation energy was adopted by the

Lazaridis-Karplus implicit solvent model, EEF1.[42] The distance- and angular-dependent hydrogen bond interaction was modeled using a reaction-like algorithm.[43] Screened electrostatic interactions were computed by the Debye-Hückel approximation. A Debye length of 1 nm was used by assuming a water dielectric constant of 80 and a monovalent electrolyte concentration of 0.1 M. The Anderson's thermostat was used to maintain constant temperature.

The structural coordinates for IAPP peptides were obtained from the protein bank (PDB code: 5MGQ). For peptides and LPC, basic and acidic amino acids and nitrogen were assigned charges corresponding to their titration states at physiological condition, i.e. Arg and Lys residues were assigned +1, Asp and Glu were assigned -1, while His was neutral. Counter ions (Cl^-) were added to maintain the net charge of the systems zero and accounted for possible counter-ion condensation.

A large fibril model was constructed with 40 IAPPs forming a two-layered fibril using the solid-state NMR-derived constraints,[36] which was assigned a 1.5-degree twist between consecutive IAPP beta-sheets. Specifically, side chains of Gln10, Leu12, Asn14 and Leu16 were located inward to the beta-sheet formed by residues 28-37. The side chains of Arg11, Ala13 and Phe15 in the protofibril were buried to form the fibril (Fig. S3). Using the same proximity constraints, DMD simulations were performed to relax the model structure until the system's potential energies reached equilibrium at 300 K. As the model fibril comprised of 40 IAPP monomers, the fibril was fixed during DMD simulations of its binding with LPCs.

All simulations were conducted at 300 K. To maintain the same peptide concentration in the systems of LPC monomers and micelles interacting with peptides (molar ratios of 24:6 and 2:2, respectively), cubic simulation boxes with equal dimensions of 183.0 and 126.8 Å were used

correspondingly. The periodic boundary condition was applied in all simulations. For each molecular system, 20 independent simulations were performed with different initial inter-molecular distances and orientations to avoid bias. For data analysis, an inter-atomic distance cutoff of 5.0 Å was used to define an atomic contact.

By initially positioning linear LPCs evenly in a spherical arrangement with the tails pointing inwards and heads outwards, relaxation simulations were performed at 300 K. The equilibrated values of radius of gyration, *Rg*, were evaluated for micelles with 25 to 60 LPCs, with intervals of 5 for a total of 8 systems. Using the simple relationship between radius r and *Rg*, $r = \sqrt{5/3}Rg$, we found that 50 LPCs resulted in a spherical micelle structure of ~4 nm in diameter. The pre-formed micelle structure was used to study its effect on IAPP self-association.

ACKNOWLEDGMENT

This work was supported by ARC Project CE140100036 (Davis), NSF CAREER CBET-1553945 (Ding), NIH MIRA R35GM119691 (Ding) and Monash Institute of Pharmaceutical Sciences (Ke). Davis is thankful for the award of an ARC Australian Laureate Fellowship. Pilkington acknowledges an Australian Government Research Training Program (RTP) Scholarship.

Supporting Information

The Supporting Information includes a TEM image of LPC micelles, normalized UV circular dichroism spectra for IAPP in the absence/presence of LPC above and below CMC, and IAPP amyloid fibril structure.

REFERENCES

1. L. Haataja, T. Gurlo, C. J. Huang and P. C. Butler, *Endocrine Rev.,* 2008, **29**, 303-316.
2. P. C. Ke, M.-A. Sani, F. Ding, A. Kakinen, I. Javed, F. Separovic, T. P. Davis and R. Mezzenga, *Chem. Soc. Rev.,* 2017 (DOI: 10.1039/C7CS00372B).
3. J. R. Brender, K. Hartman, R. P. R. Nanga, N. Popovych, R. de la Salud Bea, S. Vivekanandan, E. N. G. Marsh and A. Ramamoorthy, *J. Am. Chem. Soc.,* 2010, **132**, 8973-8983.
4. R. P. R. Nanga, J. R. Brender, S. Vivekanandan and A. Ramamoorthy, *Biochimica et Biophysica Acta,* 2011, **1808,** 2337-2342.
5. J. L. Larson and A. D. Miranker, *J. Mol. Biol.*, 2004, **335**, 221-231.
6. M. F. M. Sciacca, D. Milardi, G. M. Messina, G. Marletta, J. R. Brender, A. Ramamoorthy and C. La Rosa, *Biophys. J.,* 2013, **104**, 173-184.
7. X. Ge, A. Kakinen, E. N. Gurzov, W. Yang, L. Pang, E.H. Pilkington, P. Govindan-Nedumpully, P. Chen, F. Separovic, T. P. Davis, P.C. Ke and F. Ding, *Chem. Commun.*, 2017. **68**, 9394-9397.
8. P. Cao, A. Abedini, H. Wang, L.-H. Tu, X. Zhang, A. M. Schmidt and D. P. Raleigh, *Proc. Natl. Acad. Sci. USA,* 2013, **110**, 19279-19284.
9. M. Duan, J. Fan and S. Huo, *PLoS One,* 2012, **7**, e47150.
10. C. Guo, S. Cote, N. Mousseau and G. Wei, *J. Phys. Chem. B,* 2015, **119**, 3366-3376.
11. Y. Porat, S. Kolusheva, R. Jelinek and E. Gazit, *Biochem.,* 2003, **42**, 10971-10977.
12. D. H. J. Lopes, A. Meister, A. Gohlke, A. Hauser, A. Blume and R. Winter, *Biophys. J.,* 2007, **93**, 3132-3141.
13. R. A. Ritzel, J. J. Meier, C.-Y. Lin, J. D. Veldhuis and P. C. Butler, *Diabetes,* 2007, **56**, 65-71.
14. S. M. Patil, S. Xu, S. R. and A. T. Alexandrescu. *J. Biol. Chem.,* 2009, **284**, 11982-11991.
15. E. Sparr, M. F. M. Engel, D. V. Sakharov, M. Sprong, J. Jacobs, B. de Kruijff, J. W. M. Hoppener and J. A. Killian, *FEBS Lett.,* 2004, **577**, 117-120.

16. M. Gao and R. Winter, *J. Diabetes Res.,* 2015, **2015**, 849017.

17. K. Sasahara, K. Morigaki and K. Shinya, *FEBS Lett.,* 2014, **281**, 2597-2612.

18. Y. Hirakura, W. W. Yiu, A. Yamamoto and B. L. Kagan, *Amyloid.,* 2000, **7**, 194-199.

19. N. Bag, A. Ali, V. S. Chauhan, T. Wohland and A. Mishra, *Chem. Comm.,* 2013, **49**, 9155-9157.

20. R. Kayed, Y. Sokolov, B. Edmonds, T. M. McIntire, S. C. Milton, J. E. Hall and C. G. Glabe, *J. Biol. Chem.,* 2004, **279**, 46363-46366.

21. C. Galvagnion, A. K. Buell, G. Meisl, T. C. T. Michaels, M. Vendruscolo, T. P. J. Knowles and C. M. Dobson, *Nat. Chem. Biol.,* 2015, **11**, 229-234.

22. E. H. Pilkington, Y. Xing, B. Wang, A. Kakinen, M. Wang, T. P. Davis, F. Ding and P. C. Ke, *Sci. Rep.,* 2017, **7**, 2455.

23. S. R. Bergmann, B. T. Jr. Ferguson and B. E. Sobel, *Am. J. Physiol.,* 1981, **240**, H229-H237.

24. T. Kishimoto, Y. Soda, Y. Matsuyama and K. Mizuno, *Clin. Biochem.,* 2002, **35**, 411-416.

25. Y. Wu, Q. Lu, J. S. Hudson, A. S. Mount, J. M. Moore, A. M. Rao, E. Alexov and P. C. Ke, *J. Phys. Chem. B,* 2006, **110**, 2475-2478.

26. R. Qiao and P. C. Ke, *Am. Chem. Soc.,* 2006, **128**, 13656-13657.

27. J. Seeliger, K. Weise, N. Opitz and R. Winter, *J. Mol. Biol.,* 2012, **421**, 348-363.

28. F. Ding, D. Taso, H. Nie and N. V. Dokholyan, *Structure,* 2008, **16**, 1010-1018.

29. D. C. Rodriguez Camargo, K. Tripsianes, K. Buday, A. Franko, C. Gobl, C. Hartlmuller, R. Sarkar, M. Aichler, G. Mettenleiter, M. Schulz, A. Boddrich, C. Erck, H. Martens, A. K. Walch, T. Madl, E. E. Wanker, M. Conrad, M. H. de Angelis and B. Reif, *Sci. Rep.,* 2017, **7**, 44041.

30. A. M. Sheikh and A. Nagai, *FEBS J.,* 2011, **278**, 634-642.

31. S. Yamamoto, K. Hasegawa, I. Yamaguchi, S. Tsutsumi, J. Kardos, Y. Goto, F. Geyjo and H. Naiki, *Biochemistry,* 2004, **43**, 11075-11082.

32. T. Ookoshi, K. Hasegawa, Y. Ohhashi, H. Kimura, N. Takahashi, H. Yoshida, R. Miyazaki, Y. Goto and H. Naiki, *Nephrol. Dial. Transplant.,* 2008, **23**, 3247-3255.

33. I. Usov and R. Mezzenga, *Macromolecules*, 2015, **48**, 1269–1280.

34. M. Wang, A. Kakinen, E.H. Pilkington, T. P. Davis and P. C. Ke, *Biomater. Sci.,* 2017, **5**, 485-493.

35. S. Sakagashira, H. J. Hiddinga, K. Tateishi, T. Sanke, T. Hanabusa, K. Nanjo and N. L. Eberhardt, *Am. J. Pathol.,* 2000, **157**, 2101–2109.

36. S. Luca, W.-M. Yau, R. Leapman and R. Tycko, *Biochem.*, 2007, **46**, 13505–13522.

37. R. Carrotta, C. Canale, A. Diaspro, A. Trapani, P. L. San Biagio and D. Bulone, *Biochemica et Biophysica Acta,* 2012, **1820**, 124-132.

38. F. Librizzi, R. Carrotta, D. Spigolon, D. Bulone and P. L. San Biagio, *J. Phys. Chem. Lett.*, 2014, **5**, 3043-3048.

39. M. J. MacDonald, L. Ade, J. M. Ntambi, I. U. H. Ansari and S. W. Stoker, *J. Biol. Chem.*, 2015, **290**, 11075-11092.

40. The Art of Molecular Dynamics Simulation | Computational Science and Modelling. *Cambridge University Press* Available at: http://www.cambridge.org/us/academic/subjects/physics/computational-science-and-modelling/art-molecular-dynamics-simulation-2nd-edition. (Accessed: 27th February 2015).

41. M. P. Allen and D. J. Tildesley, *Computer Simulation of Liquids*, Clarendon Press, 1989.

42. T. Lazaridis and M. Karplus, *Curr. Opin. Struct. Biol.*, 2000, **10**, 139–145.

43. F. Ding, J.M. Borreguero, S.V. Buldyrev, H.E. Stangley and N.V. Dokholyan, *Proteins: Structure, Function and Genetics*, 2003, **53**, 220-228.

FIGURES AND CAPTIONS

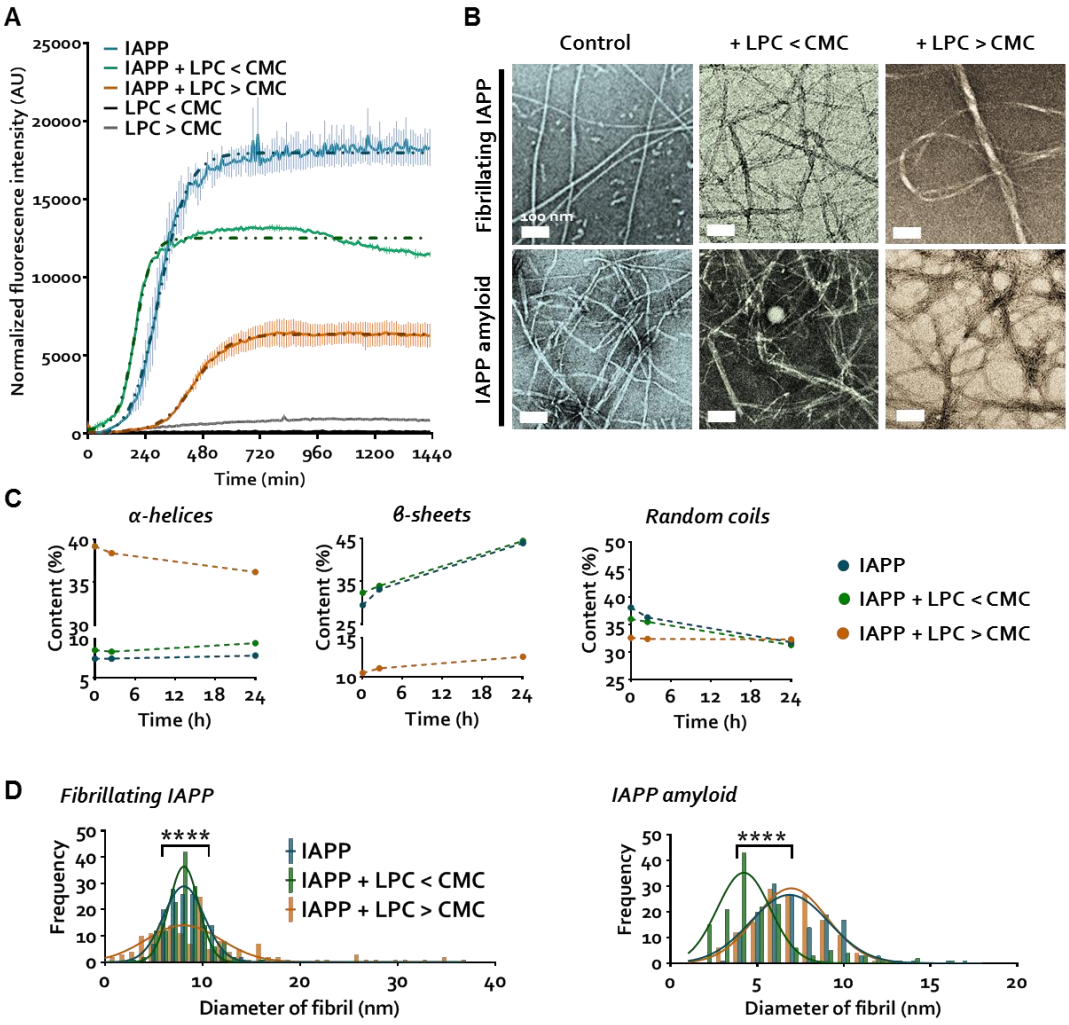

Figure 1. Effects of micellar (> CMC) and non-micellar (< CMC) LPC on IAPP fibrillation and amyloid remodelling. Concentrations of IAPP (25 μM), LPC < CMC (25 μM) and > CMC (2 mM) were fixed in all experiments. (A) ThT fluorescence assay of IAPP and LPC alone (both above and below the CMC) or as mixed samples, with sigmoidal least-squares fit (dotted lines); error = SEM. (B) TEM imaging of IAPP and IAPP amyloids after 24 h incubation with or without LPC, scale = 100 nm. (C) IAPP secondary structures in the presence and absence of LPC as determined through circular dichroism spectroscopy. Lines are intended to guide the eye. (D) Diameter frequencies of IAPP amyloid fibrils with Gaussian least-squares fit, **** $p < 0.0001$ *(one-way ANOVA with Tukey's correction)*.

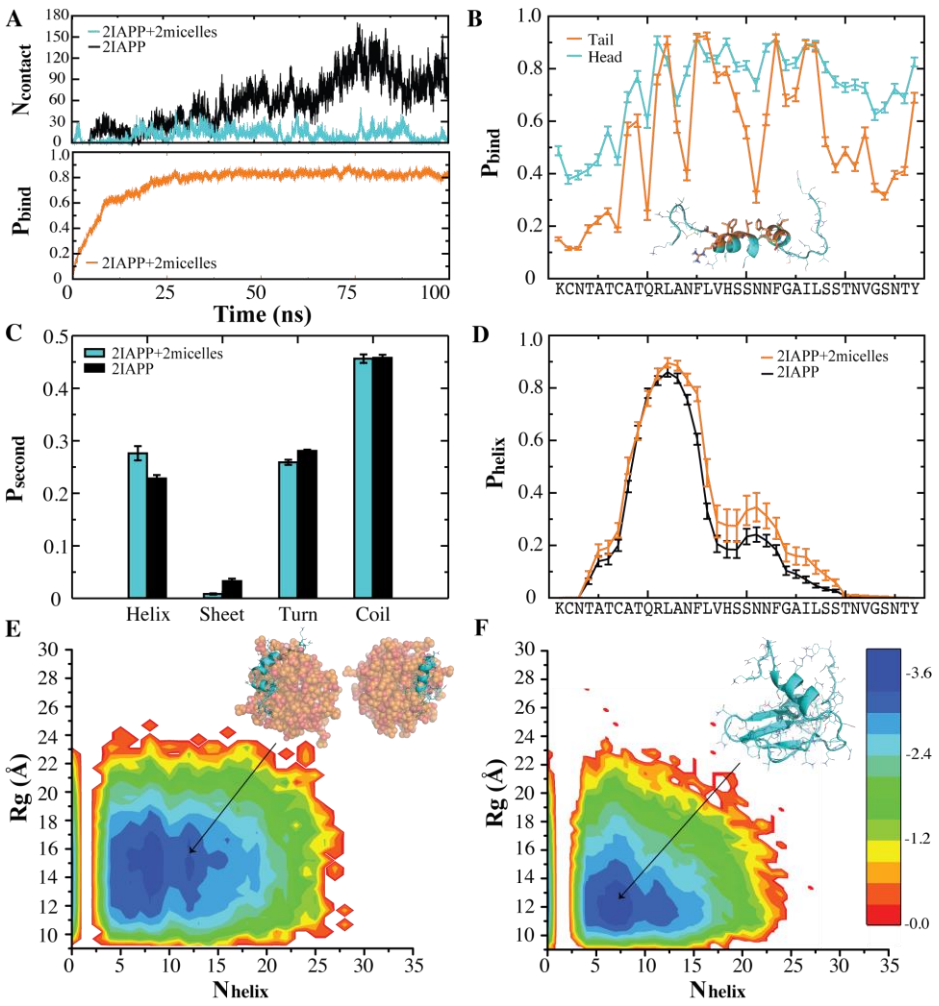

Figure 2. IAPP-LPC micelle interaction. (A) Average contact number between pair-wise IAPPs, $N_{contact}$ (top) and binding frequency between IAPP and LPC micelle, P_{bind} (lower) as a function of time. (B) Binding frequency P_{bind} of each IAPP residue with hydrophobic and hydrophilic regions of LPC micelle derived from the IAPP-LPC complexes. Residues with strong binding to the hydrophobic core of LPC micelle are highlighted as sticks in a representative micelle-bound IAPP structure (inset). (C) Secondary structure contents, P_{second}, of IAPP with and without LPC micelle. (D) The α-helix propensity P_{helix} of each IAPP residue with and without LPC micelle. (E, F) The 2D-PMF of IAPP with and without LPC micelle at T = 300 K as a function of radius of gyration, *Rg*, and the number of residues in helical conformation, N_{helix}. The typical structures corresponding to energy basins indicated by arrows are shown as inset where IAPP (cyan) is illustrated in carton and LPC micelle (orange) in spherical representation.

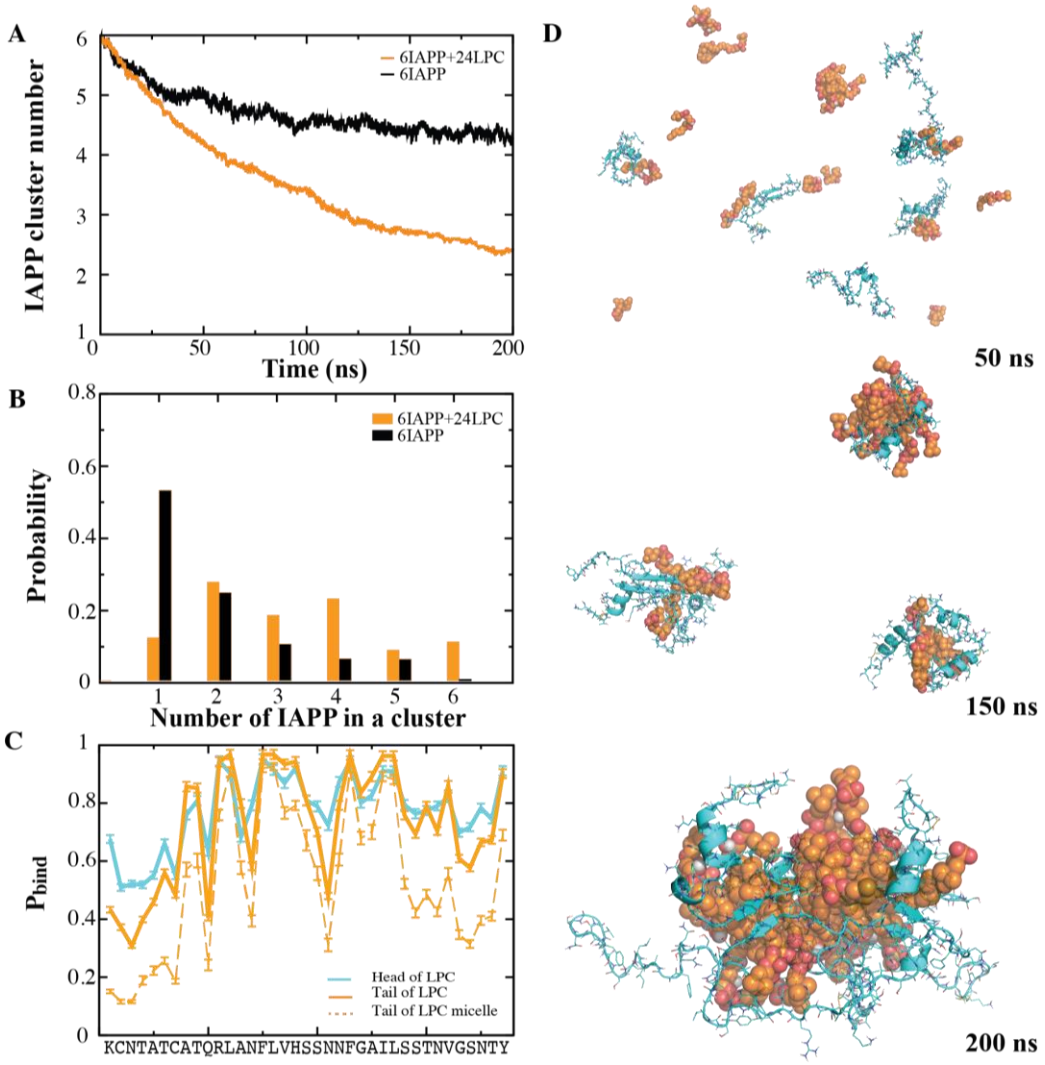

Figure 3. IAPP-soluble LPC interaction. (A) Average number of IAPP clusters as a function of simulation time in the presence and absence of LPCs. (B) Mass-weighted histograms of IAPP cluster sizes computed from the last 25 ns of corresponding simulations. (C) Binding frequency, P_{bind}, of each IAPP residue with hydrophobic and hydrophilic regions of LPC derived from the IAPP-LPC complexes. For comparison, binding with the hydrophobic region of LPC micelle is also shown as a dash line. (D) Snapshot structures along a DMD trajectory showing the co-aggregation process, where IAPPs (cyan) are in carton representation and LPCs in spherical representation.

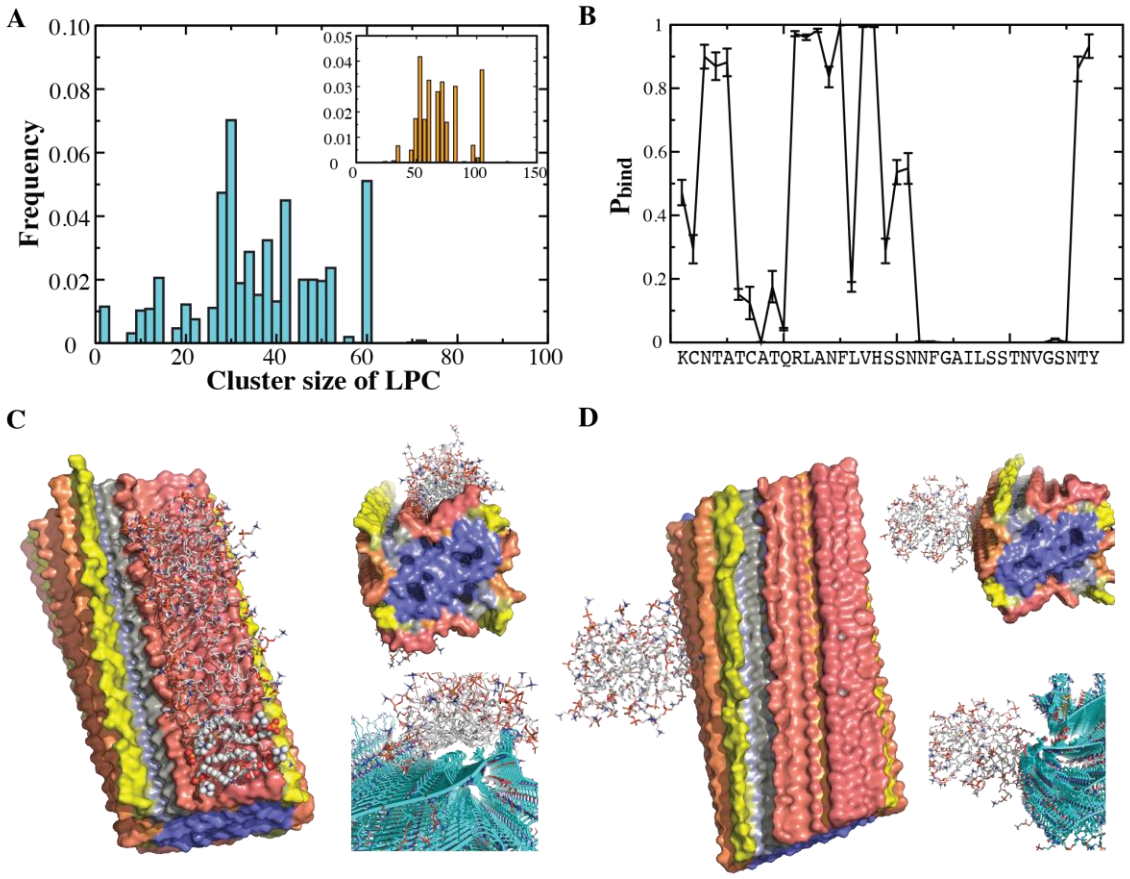

Figure 4. IAPP amyloid-soluble LPC interaction. (A) Mass-weighted histograms of LPC cluster sizes in solution and bound to fibril (inset) computed from IAPP amyloid fibril and LPC simulations. (B) Binding probability, P_{bind}, of each IAPP residue in the fibril with LPC. Two main binding sites for LPC on IAPP amyloid fibrils correspond to half-worm like (C) and micelle (D) morphologies, with the binding surfaces shown as insets. The fibril is coloured by the binding probability of IAPP residues with LPC: orange (0.7-1), yellow (0.3-0.7), grey (0.1-0.3) and blue (<0.1) indicating high to low binding probabilities. LPCs are highlighted as spherical representation in panel (C) from top view to show LPCs fit onto groves between consecutive β-strands.